LIGO SURF Project

Second Interim Report # 08072023

Estimation of the Stochastic Gravitational Wave Background from binary mergers

By Pritvik Sinhadc
Undergraduate student pursuing Bachelor of Science in Physics
The Division of Physics, Mathematics and Astronomy
California Institute of Technology
psinhadc@caltech.edu
pritvik.sinhadc@LIGO.org

Mentors:

Dr. Alan Weinstein
Professor of Physics
The Division of Physics, Mathematics and Astronomy
California Institute of Technology
ajw@caltech.edu

Dr. Patrick Meyers
Postdoctoral Scholar Research Associate in Physics
The Division of Physics, Mathematics and Astronomy
California Institute of Technology
pmeyers@caltech.edu

Dr. Arianna Renzini
Postdoctoral Scholar Research Associate in Physics
The Division of Physics, Mathematics and Astronomy
California Institute of Technology
arenzini@caltech.edu

Abstract
The ground-based International Gravitational-Wave Observatory Network (IGWN), including the Laser Interferometer Gravitational-Wave Observatory (LIGO) stations at Hanford and Livingston, Virgo and KAGRA [1], has detected gravitational waves (GWs) from Compact Binary Coalescence (CBC) sources [2] in distant galaxies as far away as 8 Gigaparsecs [3], which corresponds to a redshift of slightly greater than 1. More distant sources are too faint to be confidently detected as individual events. However, they are expected to be so numerous that they can be detectable as a Stochastic Gravitational Wave Background (SGWB) [4]. While stringent upper limits on the strength of the SGWB as a function of frequency in units of the cosmological closure density of the universe, $\Omega_{GW}(f)$ [5], have been made through the IGWN, there has been no observed detection of the SGWB as such. However, while this was overturned as per the June 28, 2023, announcement on the preliminary detection of an SGWB from supermassive black hole mergers, in particular background from stellar mass sources is still to be detected [15]. Early implications for the SGWB from the first observation of Binary Black Hole (BBH) mergers [6] and more recent models from advanced LIGO and VIRGO data [7, 8] have all provided estimates of the CBC merger rate that suggest that we are close to detection of the SGWB. The estimates from the 'Regimbau method' [6] come from complex simulations of many individual events, while the 'Callister method' [7] is based on numerical evaluation on an analytical expression for the SGWB. We reproduce these estimates through a thorough analysis of the methods used by Regimbau and Callister [6, 7] and study the degree to which they agree with each other, as well as studying the extent to which the results depend on uncertainties in the merger rate as a function of mass and redshift distributions of the sources. Overall, we investigate the predictions on SGWB parameters and constrain its limits, thereby decoding how the background changes due to uncertainties in several important variables. This incorporation of the latest theoretical models, with a key understanding of the limits and constraints in these frameworks, will aid in the long-term goal of refining estimates on the SGWB.

GW science: An introduction
The principles of general relativity, specifically the link between the spacetime metric as described by Einstein field equations and energy-momentum tensor, including matter, momentum, and stress, show that acceleration of massive objects creates warping or distortions in the fabric of spacetime. This phenomenon of spacetime curvature can propagate through space as a GW in a manner analogous to electromagnetic or even fluid waves spreading out from a source [2].

All GWs that have been detected by the IGWN to date are attributed to CBCs [3], specifically the merger of compact, stellar mass objects [1]. These include events like merger of stellar mass objects [3], such as two neutron stars or two black holes [3], or a black hole and a neutron star [1, 3]. During such events, a portion of the mass energy and kinetic energy of the merging objects is converted into GWs, which emanate from the merging site and progressively reduce in amplitude. Analogous to conventional waves, these GWs carry information on the original source via frequency, wavelength, and amplitude [1]. According to general relativity, it is worth noting that GWs warp space-time as they propagate due to the fundamental interplay between spacetime curvature, matter-energy distribution, and momentum.

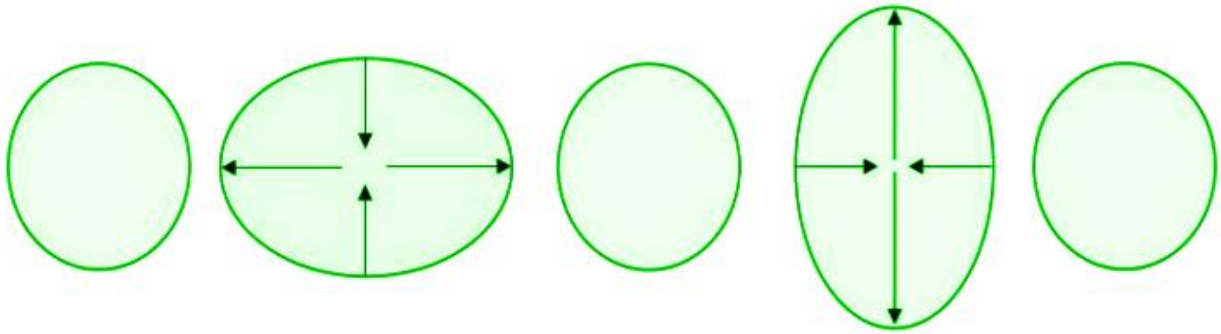

Figure 1: This figure illustrates the deformation of the space-time fabric within an object induced by the passage of a GW, with each image representing a distinct stage in the warping. The object oscillates from maximum longitudinal stretching to maximum latitudinal stretching, with arrows showing the direction of warping of the spacetime fabric. Such a warping is described as linearly polarized. In this case, the effect is exaggerated, since by the time such waves are detected by the IGWN, the warping caused by them results in extremely small changes in distance — less than 1/1000th the diameter of a proton [2].

Source: Image generated by the author.

This present overview holds significance owing to the fact that the majority of the SGWB is anticipated to emanate from a superposition of CBC events [5]. To elucidate the characteristics or nature of the SGWB, it is imperative to consider the properties of such events as described above [2].

The SGWB: An overview

The SGWB is a complex amalgamation of multiple sources of GWs that offer valuable insights into the evolution and history of astrophysical collisions over the universe's timespan [4]. Although numerous theorized sources, including cosmic strings, primordial black holes, etc, have been suggested to contribute to the SGWB, the vast majority of this background is expected to originate from a superposition of sources that are fully describable with parameterized models, CBCs, along with less predictable, unmodeled bursts such as core-collapse supernovae [4, 5]. This component of the SGWB is the astrophysical background, and is expected to be made up of the superposition of numerous GW events throughout the universe's history [4, 5]. A much smaller component of the SGWB consists of a cosmological background, including the GWs predicted to be formed immediately after the Big Bang through processes such as the preheating phase at the end of Cosmic Inflation, and GWs generated during inflation [11, 12, 13]. Other hypothesized sources include baryonic acoustic oscillations, or even further back with contributions from earlier phase transitions [4]. Although this portion of the SGWB is fainter, we note that its frequency lies beyond the detectable range of the ground-based GW detectors, which encompass a frequency of 20-20000 Hz [11, 12, 13] and some of the advanced GW experiments, such as Laser Interferometer Space Antenna (LISA) or even the Pulsar Timing Array (PTA) [9]. Thus, this report focuses solely on the astrophysical component from CBCs.

The SGWB is expected to be fundamentally stochastic in nature with a source distribution assumed to be isotropic, as well as being randomly distributed across the observable universe

[10]. An alternate anisotropy, that of a background centered around local galaxy superclusters, is also discussed later in this report.

The SGWB: Expected detection signature

It is important to note that the signal of the SGWB is indistinguishable from detector noise arising out of ground systems such as LIGO. This is shown in the figure below, wherein the stochastic signal is enclosed within a higher amplitude noise. Cross correlation between detectors is needed to extract useful parameter information on the SGWB. Figure 2, presented below [10], depicts a prototype of the stochastic signal anticipated to resemble the SGWB.

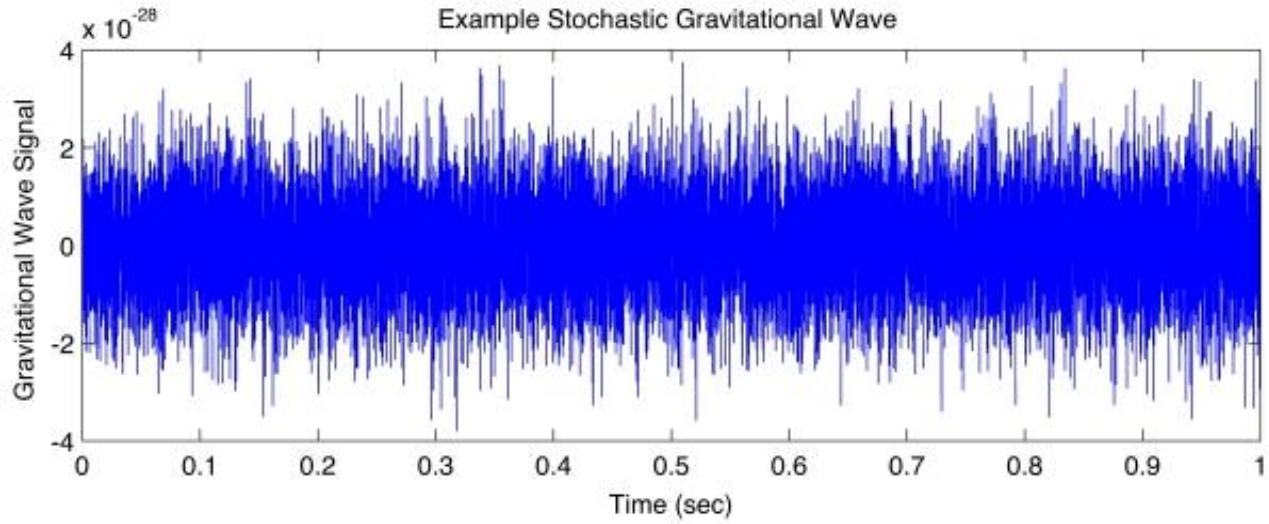

Figure 2: An example of a signal from a stochastic GW source. The signal is roughly uniform in amplitude and frequency in time, and is very faint [10].

Source: LIGO Scientific Collaboration [10]

While Figure 2 above shows the overall expected signal that would be observed in the event of an SGWB detection, we can also simulate the power spectral density of the expected signal (power of the signal with respect to frequency), as well as key components, like the actual line representing how the power of the SGWB changes over frequency, how the power of noise changes with respect to frequency, and how the power of the data points change over frequency [12]. A simulated image is shown in Figure 3 below using the pygwb module for GW science in python as well as matlab [12]. However, we also note that there are some discrepancies in the simulated results obtained from pygwb. In particular, the graph in Figure 3 represents the injection of a broken power law into noise data. Hence, the actual scale of the PSD does not match the actual PSD of an SGWB [12]. Moreover, in reality, we do not actually expect to see any data below 15 Hz or 20 Hz. This may cause the higher portion of the graph in Figure 3, which we would not expect in reality as shown below. In any case, we can still see the very rough shape of the PSD of an SGWB in Figure 3 below.

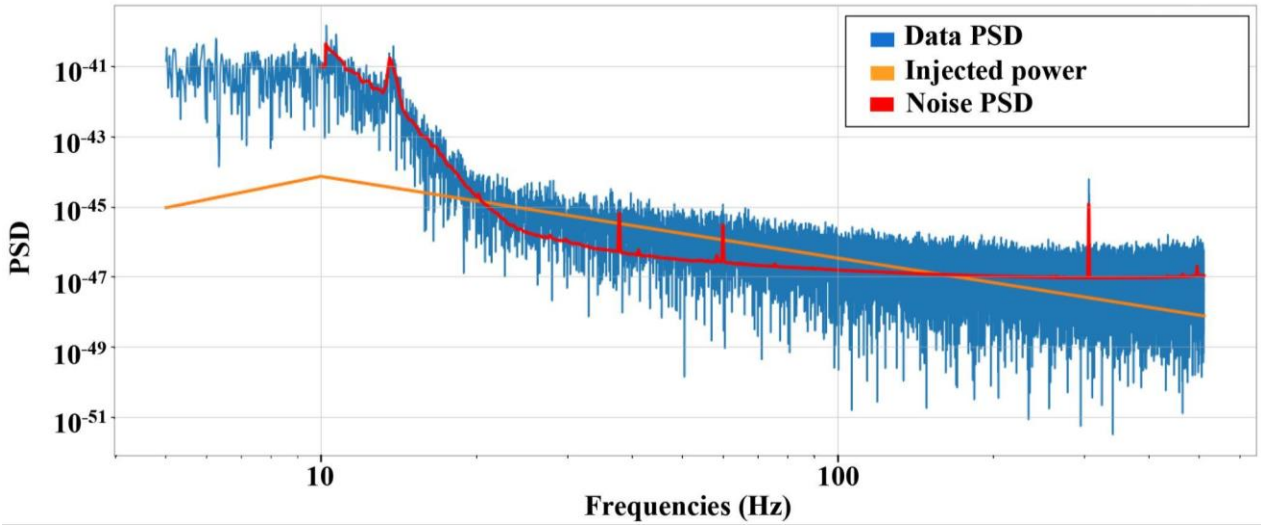

Figure 3: Visualizing the data PSD (shown in blue), an injected curve representing the broken power law (shown in orange), and the original noise curve (shown in red). This graph identifies the final result after injecting a broken power law into the LIGO noise data, and is emblematic of the PSD signature, which we may expect with a SGWB within noise data. Here, the signal we inject is a broken power law spectrum — or a power law that reaches a peak and 'breaks', and then decreases afterward [12]. However, since the above graph is an example, the broken power law is shown for illustrative purposes [12]. In reality, we would expect the peak to be much farther along the frequency axis — not at 10 Hz.

Source: Image generated by the author. However, the overall process to generate the above image can be found in tutorials in the original pygwb documentation [12].

It should also thus be noted that one of the first steps we take to analyze a simulated SGWB is to look at its energy density, which can be derived from the PSD, and is dependent on merger rate, mass distribution, and the evolution of the prior two values with redshift. This is because we expect the merger rate to peak during (or after) 'Cosmic Noon', when the star formation rate of the universe was at its maximum, at a redshift of approximately 2 [16]. We also do not expect any mergers to occur before 'Cosmic Dawn' or when the first stars were born [16]. Observed merger rate is in principle predictable under assumption mergers following the birth of binary systems, which are birthed around when individual stars form; star formation rate tells us this up to high redshift. Thus, we can predict that the energy density of the SGWB appears as a broken power law (as shown in Figure 3 above). A more detailed derivation and explanation is given later, but the expected signal PSD is shown in Figure 4 below:

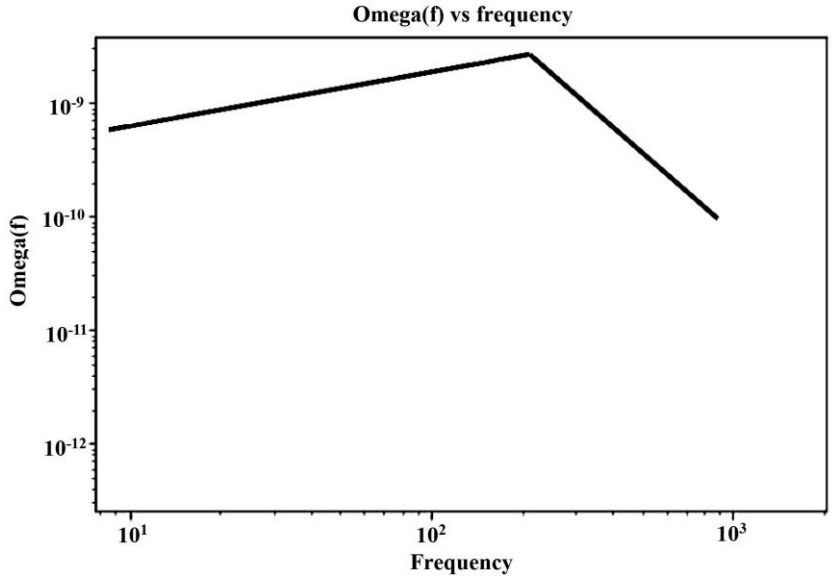

Figure 4: A closer look at an example of broken power law representing a signal PSD from a hypothetical stochastic signal over a frequency distribution that we may expect [12].

Source: Image generated by the author. However, the overall process to generate the above image can be found in tutorials in the original pygwb documentation [12].

Motivation: Constraining the parameters of SGWB

GWs convey vital information on their sources, and likewise, the SGWB provides valuable insights into the underlying population of astrophysical sources that constitute it, including their mass distribution, the rate of formation of CBCs, and other parameters [5, 6]. Thus, by simulating SGWB with changing parameters, including amplitude, spectral shape, and angular distribution of sources, a novel window to understand the evolution of CBCs can open, targeting new, in-depth insights on how mass distribution of compact binary systems and their isotropy and redshift distribution impact the SGWB, which potentially reveal further insights into the astrophysical origins of GWs [14].

The primary motivation for our endeavor to compare the differing methods of simulating SGWBs is to further constrain the expected detection of such a background and understand the new insights that can be gathered on the evolution of CBCs over cosmic time. Currently, due to relativistic numerical simulations estimating parameters of the SGWB, as well as new estimates generated by the LIGO, VIRGO, KAGRA (LVK) detectors, we have constrained the limits of the SGWB [6], the expected signal to noise ratio (SNR) needed for detection, and the mean expected energy density of the background. The results can be summarized in Figure 5 below.

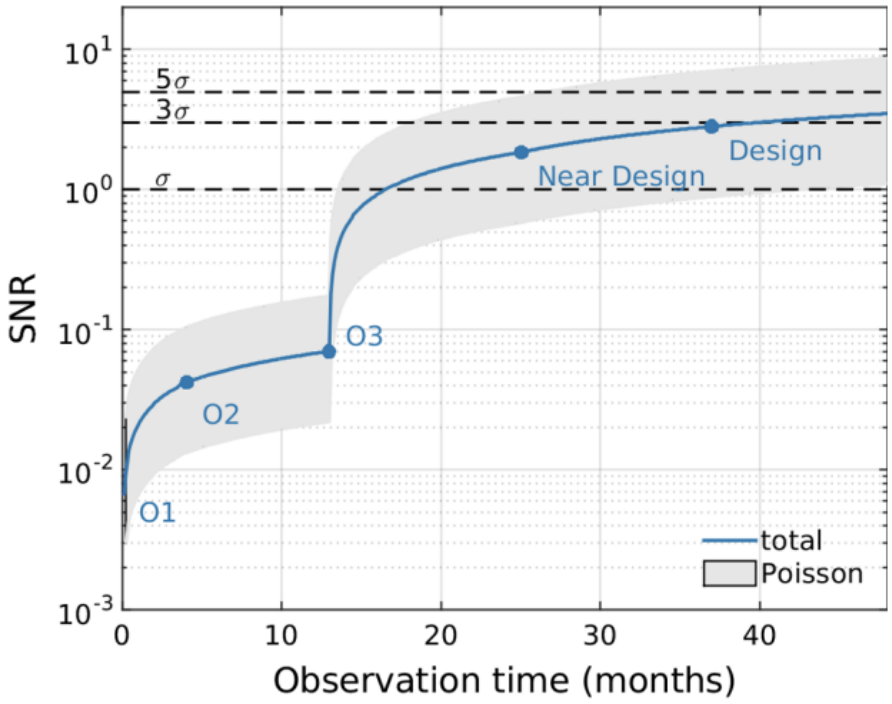

Figure 5: The image above shows the improvements in detector SNR (ratio of signal power to noise power or signal to noise ratio) [6]. As measured SNR increases, the sensitivity level of the SGWB will also be reached by the LVK network [6]. Therefore, overall, given the energy densities that can be measurable by upcoming detectors is also taken into account, it is clear that we might be in a position to detect the SGWB within a few years. The result of this research project, hence, contributes to further constraining and understanding of the methodologies used to construct predictions of the SGWB, as well as decode the range of possible predictions from simulation [6].

Source: Fig 1 (right), GW170817: *Implications for the Stochastic Gravitational-Wave Background from Compact Binary Coalescences,* B. P. Abbott et al, (LIGO Scientific Collaboration and Virgo Collaboration), *Phys. Rev. Lett*, 120, 091101, Published February 28, 2018, https://journals.aps.org/prl/abstract/10.1103/PhysRevLett.120.091101

This research project aims at investigating the properties of the SGWB resulting from CBCs, with a focus on how different variables such as mass distributions, anisotropies, and redshift distributions impact the background signal. To accomplish this, the simulation techniques employed to model the SGWB are analyzed in detail, including how such models can be parametrized to account for different variables [6, 7]. The theoretical framework for modeling the SGWB is developed, including understanding the power spectrum of strain fluctuations generated by the sources, along with a replication of the numerical simulations utilized to generate background signals for different scenarios [6, 7].

More specifically, the simulations are used to investigate the properties of the SGWB due to different mass distributions of CBCs. The impact of anisotropies in the distribution of CBC

sources on the SGWB has also been studied. Additionally, this research project examines the impact of redshift distributions on the SGWB due to CBCs. This includes investigating the potential for the SGWB to be affected by the evolution of the universe over time.

Overall, the goal of this research project is to gain a deeper knowledge of the SGWB due to CBCs and the information it carries about the population of astrophysical sources that compose it. By studying how different variables impact the SGWB, we hope to develop a better theoretical framework for modeling the background signal, which is crucial for interpreting future observations of the SGWB, and will aid in the overarching goal of gaining a better understanding of what to expect when the SGWB is finally detected.

Mathematical Background for SGWB

The SGWB is Gaussian (normally distributed), unpolarized compared to an individual source and is expected to be isotropic in nature — or invariant with respect to direction of measurement [11]. This background can be fully characterized by the background energy density, and this spectrum can be expressed, as mentioned previously, by the term $\Omega_{GW}(f)$. This term allows for the calculation of the GW energy density within a frequency interval [11]. Specifically, $\Omega_{GW}(f)$ can be described by the equation below [11]:

$$\Omega_{GW}(f) = \frac{f d\rho_{GW}}{\rho_c df} \quad (1)$$

Where $d\rho_{GW}$ is GW energy density, df the frequency interval, ρ_c the critical energy density needed to have a flat, non curved Universe — calculated as below:

$$\rho_c = \frac{3H_0^2 c^2}{8\pi G} \quad (2)$$

Where c is the speed of light, G is Newton's gravitational constant, H_0 is Hubble constant, which we take from Planck satellite data as 67.4 km/s/Mpc [11].

Equation (1) for $\Omega_{GW}(f)$ derives a relationship between the energy density of the SGWB and the frequency content, thereby allowing us to understand the contribution of GWs for specific frequency intervals [11]. The frequency f that we measure in equation (1) above is of course the frequency measured by a detector. If we take f_{source}as the frequency as observed from source frame [11], we can decompose our equation (1) into another form below:

$$\Omega_{GW}(f) = \frac{f d\rho_{GW}}{\rho_c df} = \frac{f}{\rho_c}\int_0^{10} \frac{R_m(z)dE}{(1+z)H(z)df_{source}}dz \quad (3)$$

In equation (3) [11], we still measure energy density of GWs within the frequency interval for the SGWB, but we now have $\Omega_{GW}(f)$ in terms of new parameters. $R_m(z)$ is the merger rate [11] in $\mathrm{Gpc}^{-3}\mathrm{yr}^{-1}$, which is explained in further detail later on. The term f_{source} is described by the equation $f = \frac{f_{source}}{1+z}$, wherein once again f is frequency in observed frame, and f_{source} is frequency in the source frame [11]. The parameter $H(z)$ is the Hubble expansion rate [11]. Notice that each parameter described (and the integral as a whole) is in terms of z, or the redshift. Typically, we assume that CBCs occur from a redshift of twenty (corresponding to the expected time in the universe's history when the first black holes are expected to form) till now [11].

Thus, from equation (3), we have a preliminary link between the energy density of the SGWB, the redshift distribution that we are observing, as well as the mass distribution of CBCs, which the merger rate is dependent upon [11]. Therefore, the overall aim of this research has been to recontextualize these equations through simulations. By creating simulations of the SGWB using mathematical models, such as the equation (3) above, we can manually adjust the merger rate through mass distribution, redshift distribution, etc. We can see the impact of variations in parameters to the energy density of the SGWB itself. The term $\Omega_{GW}(f)$ is the background energy density of the SGWB, and is characterized by integrating the spectral energy density of the SGWB or $\frac{dE}{df_{source}}$ [11]. It is a key quantity in the study of the SGWB, and is, therefore, used to calculate the energy density and SNR of the SGWB as it provides crucial insights into the properties of the GW sources that contribute to the SGWB background [11].

Computational methods

This study of the astrophysical SGWB relies on various tools, including numerical integration, specifically of the model used in equation 3, simulations of several gravitational wave events to construct coarse-grain example SGWBs to be generated, and dedicated Python packages, particularly pygwb — the latest released version — for all of the aforementioned gravitational wave science. Numerical integration techniques can be used to better understand the spectral energy density of the SGWB, and generate predictions on sensitivity ranges of various detector and mission operations to observe the presence of an SGWB. Therefore, such techniques remain a critical tool for the final stages for this research. The result of applying these methods on the energy density $\Omega_{GW}(f)$ — as defined by equation 3 — can be seen in Figure 6 below [8].

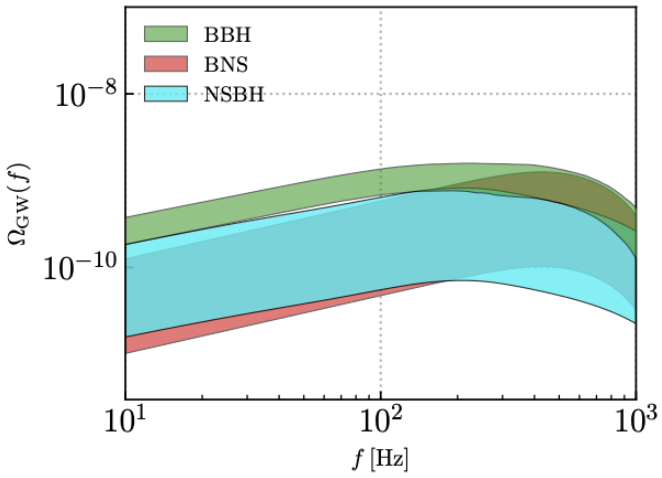

Figure 6 (left)

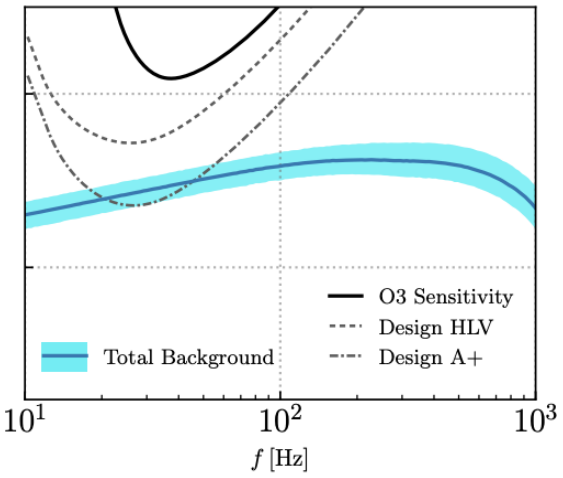

Figure 6 (right)

Figure 6: The image above shows the predictions of the SGWB due to CBCs as well as LVK detector sensitivity following Observation Run 3 [8]. Figure 6 (left) shows the expected contributions to the background from various astrophysical sources of gravitational waves, including binary black holes in green, binary neutron stars in red, and neutron star black hole mergers in blue [8]. Figure 6 (right) shows the intersection between detector sensitivity and required parameters needed to reach the SGWB detection sensitivity [8]. A key part of this

research includes understanding the appropriate uncertainty in merger rate and mass distribution for each source of the CBC SGWB.

Source: *The population of merging compact binaries inferred using gravitational waves through*, GWTC-3, B. P. Abbott et al, (LIGO Scientific Collaboration and Virgo Collaboration), February 23, 2022, https://arxiv.org/abs/2111.03634, section X and Fig 23.

The other key tools that have been used during this research is simulations based on the utility provided by Python packages for gravitational wave science, particularly pygwb [12]. Through simulations and coding, the project aims at utilizing different parameters and approximations for both mass distributions and redshift distributions in my research, apply statistical techniques to prototype SGWBs generated, study SNRs required to probe such backgrounds, etc.

Summary of objectives

The main objectives of this project are a final report, presentations, and a co-authored paper, etc:
1. Reproducing and comparing the estimates of the CBC merger rate and the SGWB from [6] and [7], which are based on different approaches, including simple simulations of individual events and numerical evaluation of analytical expressions for the SGWB.
2. Investigating the degree to which these estimates agree with each other and the implications of any discrepancies.
3. Studying the dependence of these estimates on uncertainties in the merger rate as a function of mass, redshift distributions of the sources, and potential anisotropies in overall source distribution.
4. Assessing the impact of these uncertainties on any potential constraints that could be applied to the SGWB, including the energy density of the SGWB, contributions from different mass ranges of CBCs per frequency band, etc.

Progress report

Let us calculate and graph $\Omega_{GW}(f)$ over frequency as in [7]. To do this, we have followed the method utilized by Callister to simulate the background. We start by revisiting equation 3 derived in the background section [11]. This equation shows how the calculation of $\Omega_{GW}(f)$ or the background energy density of the SGWB depends on $R_m(z)$ or the merger rate, f_{source} or frequency in source frame, and f or frequency in observed frame, where $f = \frac{f_{source}}{1+z}$, z being redshift of source [11]. $\Omega_{GW}(f)$ is characterized by integrating the spectral energy density $\frac{dE}{df_{source}}$ and allows for the calculation of the GW energy density within a frequency interval [11]. As mentioned earlier in the report, other important terms include $H(z)$ or the Hubble expansion rate, and ρ_c or the critical energy density needed to have a flat, uncurved Universe [11].

$$\Omega_{GW}(f) = \frac{f d\rho_{GW}}{\rho_c df} = \frac{f}{\rho_c}\int \frac{R_m(z)dE}{(1+z)H(z)df_{source}}dz \quad (3)$$

We can further decompose this equation by noting that $\frac{dE}{df_{source}}$ or the population averaged energy spectrum can be described as follows [17]:

$$\langle\frac{dE}{df_{source}}\rangle = \int dm_1 dm_2 \frac{dE}{df}(m_1, m_2; f(1+z))p(m_1, m_2) \quad (4)$$

Here, m_1, m_2 represent the masses of the two merging objects, and $p(m_1, m_2)$ represents their population probability distribution, dependent on their respective mass [17]. Moreover, we can also break down the merger rate distribution describing it as an integral over a time delay distribution as described below [17]:

$$R_m(z) = \int dt_d R_*(z_f(z,t_d)) F(Z < Z_c, z_f(z,t_d)) p(t_d) \quad (5)$$

Thus, we see that the merger rate depends upon the time delay distribution $p(t_d)$, redshift values z, depending on frequency, the critical redshift or z_f and Z_c, as well as the formation redshift at the critical redshift or $F(Z < Z_c, z_f(z,t_d))$ [17]. Now that we have decomposed both $R_m(z)$ and $\langle \frac{dE}{df_{source}} \rangle$, we can start reproducing the method utilized for calculating and plotting $\Omega_{GW}(f)$ as used in [7, 17]. This process is the same as used in acquiring Figure 5 of [7] and a guide for following the path to calculating and graphing $\Omega_{GW}(f)$, which can be found in [17].

To give a brief overview of the process, which is described in [17] and the final result of which is represented in [7], we create a grid of (m_1, m_2) data values, and of frequency and redshift values, respectively [17]. We can then precompute the spectral energy density for each combination of mass values, redshift of each source, and frequency of each signal [17]. Thereafter, for a given mass distribution, we can calculate the probabilities of that distribution over the mass grid [17]. Finally, we can get a precomputed grid of binary formation rates (or rate of formation of CBC systems dependent on system mass) using an assumed star formation rate R_* [17]. This grid is a function of merger redshift as well as time difference between binary system formation and merger or time delay [17]. We can also get a probability distribution of time delays, as inspiral times in such CBC systems are dependent on masses of the two objects in question [17]. To simplify the process further from here, we can get a merger rate of compact binaries from matrix multiplying our array of formation rates by a probability distribution of delay times [17].

Note, for actually encoding $\Omega_{GW}(f)$, we can summarize the above by the following steps [17]: We first define a local merger rate and mass distribution, set up the $\Omega_{GW}(f)$ object, and then reweight it according to the mass distribution in order to integrate over the range of possible object masses [17]. We then compute $\Omega_{GW}(f)$ through a function taking into account mass distribution, local merger rate, evolution of merger rate with redshift, and frequency range over which we define $\Omega_{GW}(f)$ [17]. Overall, we calculate $\frac{dE}{df_{source}}$ over the entire frequency range to get $\Omega_{GW}(f)$[17].

In totality, we provide the calculation of $\Omega_{GW}(f)$ by the following matrix product expression below [17]:

$$\Omega_{GW}(f) = \frac{f d_{\rho GW}}{\rho_c df} = \frac{f}{\rho_c} \int \frac{R_m(z) dE}{(1+z) H(z) df_{source}} dz = \frac{f}{\rho_c} \sum_z \left\{ \frac{R_m(z)}{(1+z)H(z)} \right\}_z \left\{ \langle \frac{dE}{df} \rangle \right\}_{f,z} \quad (6)$$

Where $\left\{ \langle \frac{dE}{df} \rangle \right\}_{f,z}$ is the population averaged energy spectrum dependent on frequency and redshift, and the curly brackets represent a matrix multiplication between the aforementioned grids we created [17]. Therefore, the energy density, $\Omega_{GW}(f)$, of the SGWB, or measured by a stochastic search, is described by a weighted integral over the CBC merger history over the universe's evolution and is sensitive to the totality of past mergers [17]. We can tune the minimum and maximum values of masses for neutron star binary mergers and black hole binary mergers with an assumed merger rate to arrive at plots of $\Omega_{GW}(f)$ over time, as shown in Figure 7 below [17]:

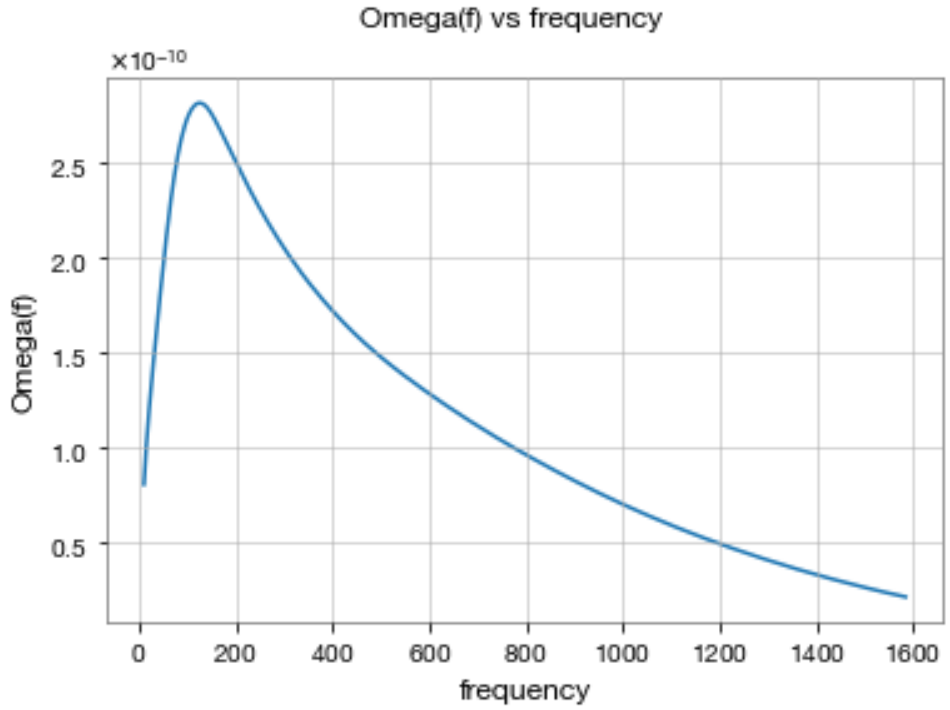

Figure 7: For the above plot, we have taken a minimum black hole mass of 5 solar masses and a maximum black hole mass of 100 solar masses, a minimum neutron star mass of 1.5 solar masses and a maximum neutron star mass of 2.5 solar masses [17]. Note, the peak in the energy density is in the hundreds of Hz, and the fact that $\Omega_{GW}(f)$ is a broken power law distribution, is reflected as predicted. Thus, we have plotted the energy density of a simulated SGWB [17].

Source: Image generated by the author, but the methodology used can be found through [7, 17].

We can also do a test to see if the SGWB plot is in reality the same as we expected. In particular, we can test the prediction that if we increase the mass distribution by increasing the maximum mass value in the merger, we should see the graph shift to lower frequencies. Figure 8 below shows exactly this.

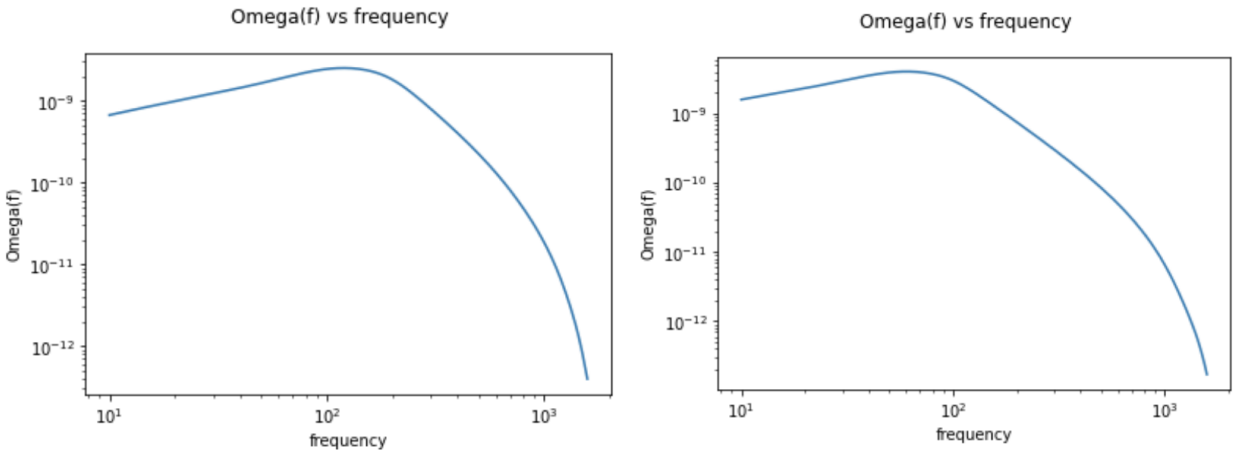

Figure 8 (left) **Figure 8 (right)**

Figure 8: Here, we use the Callister method to plot Log-scale graphs for different mass distributions. On Figure 8 (left) we see a plot for a peak in 50 solar masses for the mass of one merging object. On Figure 8 (right) we see a plot for a peak in 100 solar masses for the mass of one merging object [17]. We can see that the peak of the 100-solar-mass maximum plot is shifted to lower frequencies, which is exactly what we expect when we simulate higher mass distributions [7].

Source: Image generated by author, but the methodology used can be found through [7, 17].

Thus, the Callister method creates plots as per our predictions. More specifically, if we keep the maximum mass of both merging objects equal to one another (for one-to-one ratio of mass for the merging objects), and vary the maximum merging mass value, we can plot how frequency changes with mass distribution across several different mass values. The Callister method has m_1 and m_2 maximum values representing both merging objects. If we keep increasing these values and repeating the graphs, and from there plot how frequency varies with maximum mass, we get Figure 9 as shown below.

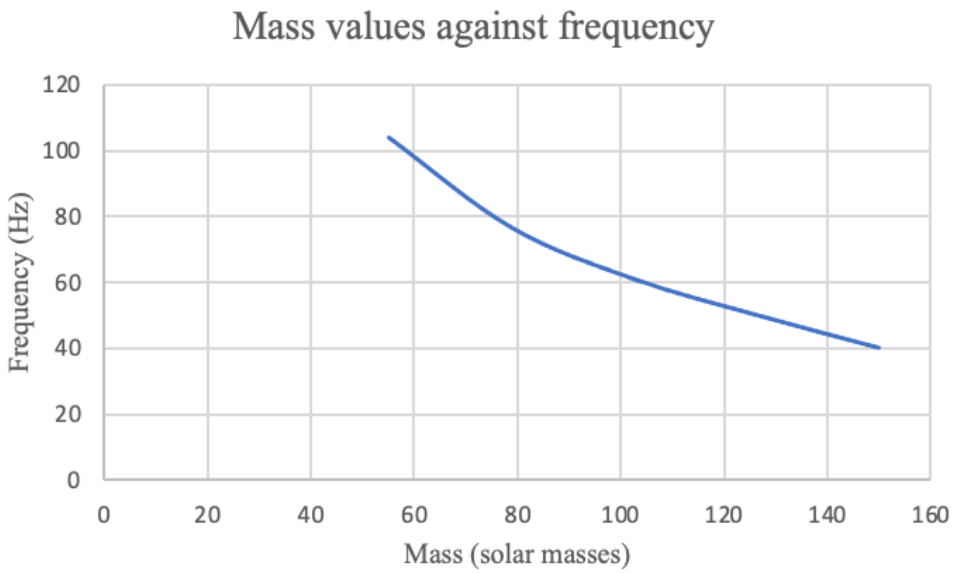

Figure 9: Here we see a linear scale plot for how peak frequency changes with mass distribution. In other words, we observe how the peak of the graph from Figure 7 changes with mass distribution. It is clear that with increasing mass distribution, by inclusion of higher and higher maximum merging masses as shown on the x axis, the frequency is shifted to lower and lower values [7, 17]. The maximum merging mass represents the maximum mass expected for m_1 and m_2 in mergers.

Source: Image generated by the author, but the methodology used can be found through [7, 17].

It should be noted that this result is dependent on several factors, especially if the local merger rate assumed in the Callister method remains constant. For Figure 9, we assume that the merger

rate remains constant. However, the mass distribution at each merger has been changed, thus leading to the plot shown above in Figure 9. However, more refined plots will need to be generated to replicate the result shown in Figure 9, as it is still unclear whether or not we expect such a wide variation in frequency range from this particular variation in maximum mass distribution. More research is needed on understanding how the merger rate function R_m also depends upon mass as an integral over mass distribution.

If we take the local merger rate (or merger rate at our current redshift), we can change this value to see how it impacts $\Omega_{GW}(f)$ across a frequency range. This result is shown in Figure 10 below. Note that for this analysis, we have chosen specific fixed merger rates to see how measurement uncertainties may affect the plots.

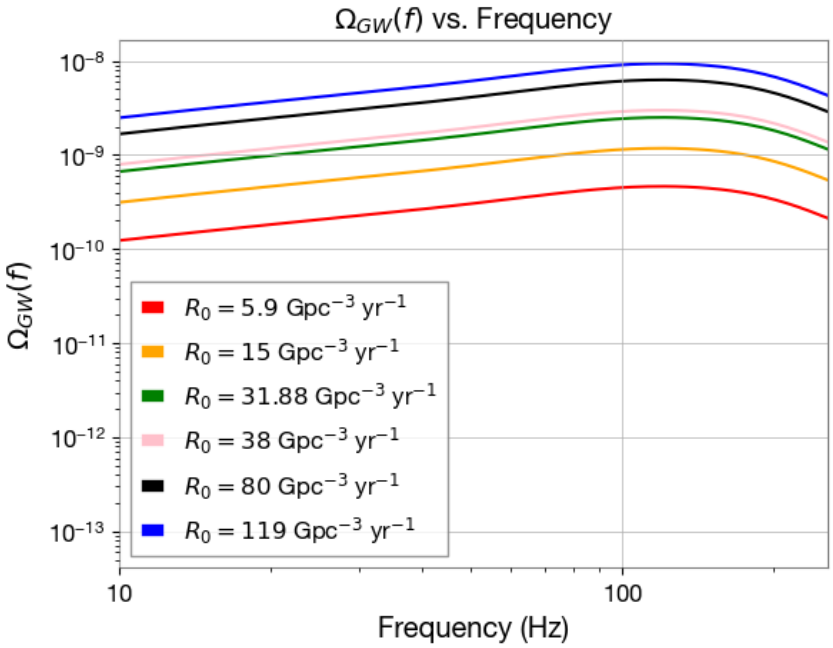

Figure 10: A plot of how $\Omega_{GW}(f)$ against frequency changes with different mean local merger rates. The graph is shifted to higher values of $\Omega_{GW}(f)$ when greater merger rates are applied — an expected outcome — as $\Omega_{GW}(f)$ represents the energy density of the SGWB. If the rate of mergers is higher, then the energy density of the SGWB is higher as well [7, 17].

Source: Image generated by author, but the methodology used can be found through [7, 17].

Now, we can also do the same calculation as described in [7,17] and plot for $\Omega_{GW}(f)$, but use a different method [18]. This is the process as outlined in [6]. This method utilized by Regimbau, and later simplified and standardized by Renzini, is Monte-Carlo-based unlike the Callister method [18]. The brief overview of this methodology is that it aims at using a Monte-Carlo sampling of individual injections of CBC events from a calculated distribution to build up $\Omega_{GW}(f)$ across a frequency range [18]. In other words, a list of CBCs is created with random parameters from a given set of Bayesian priors, including prior probability of masses, luminosity distance, etc [18]. Then corresponding time domain waveforms are injected into this simulated data representing the Hanford and Livingston LIGO detectors [18]. Finally, the total injected

$\Omega_{GW}(f)$ can be computed through the frequency domain [18]. The overall goal is to compute $\Omega_{GW}(f)$ through the injection of individual CBC events [18]. We can increase the number of injections, thereby resulting in a smoother curve, and then for each injection we can generate a parameter dictionary, a frequency domain waveform, orientation factor, and ultimately arrive at the final PSD of the signal, which is then added to the $\Omega_{GW}(f)$ spectrum [18]. The injections are sampled via Monte-Carlo methods. Thus, we can again calculate $\Omega_{GW}(f)$ as shown in Figure 11 below [18]:

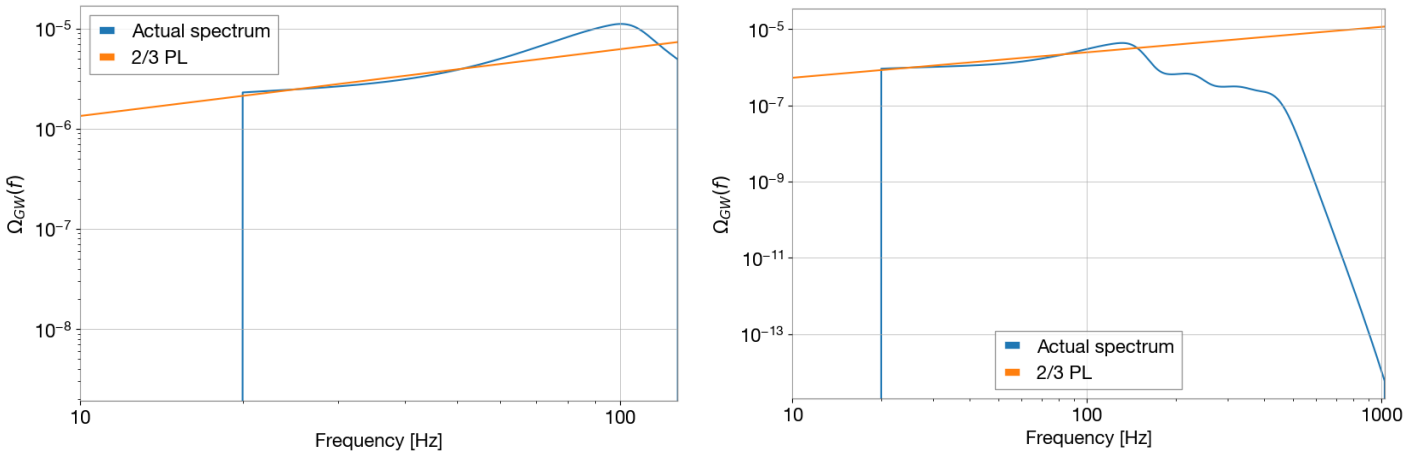

(Left) **(Right)**

Figure 11: $\Omega_{GW}(f)$ over a frequency range compared to a power law of ⅔ [18]. The priors that we specify are the average ratio of the masses in CBCs, the average masses themselves, luminosity distance, and a host of other variables [18]. If we set all other variables to 0, luminosity distance to a power law function with a minimum of 100 Mpc to 1000 Mpc, we can get the above Figure 8 (left and right) through an average mass ratio of 1.0, setting both priors for mass 1 and mass 2 to uniform distributions with a minimum of 1.5 and a maximum of 100 solar masses [18]. Note that 10 injections were used to create Figure 8 (left and right) above, which is why the graph $\Omega_{GW}(f)$ begins to become more stochastic at higher frequencies [18].

Source: Images generated by the author, but the methodology used can be found through [18].

To solve the issue of excess fluctuations in the graph, we can increase the number of injections to 100 [18]. This ensures that there are fewer gaps in the data at higher values of frequency [18]. If we keep all values the same as in Figure 8 above, but increase the number of injections to 100, we get Figure 12 below [18]:

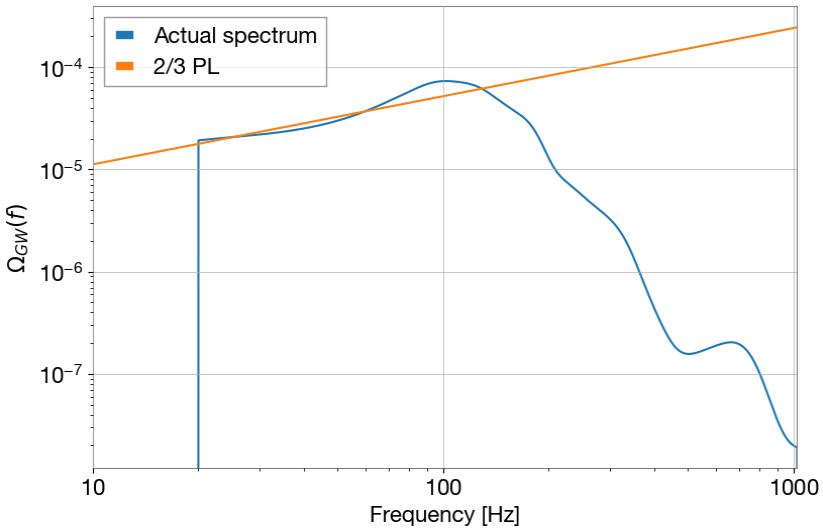

Figure 12: Using the same parameter priors in Figure 11, with only 100 injections, we can get a smoother curve [18]. Note, that each peak corresponds to some important contribution towards $\Omega_{GW}(f)$ [6]. Thus, a crucial aim for future research lies in analyzing the distribution of peaks with different parameters or prior inputs [18].

Source: Image generated by the author, but the methodology used can be found through [6, 18].

We can further witness the drop in stochasticity if we move to greater injections. We consider hyperparameters such as chirp mass as uniform distribution from 2 to 30 solar masses, a luminosity distance from 100 Mpc to 1000 Mpc with 1000 injections to generate Figure 13 below. We also note that each number of injections takes different times to run, with 10 injections taking around ten seconds, 100 injections taking around a minute, and 1000 injections taking around five minutes. More research may need to be done to see exactly what is being generated with each injection so as to understand the time taken to create the data that needs to be plotted, thereby improving time taken to generate injections.

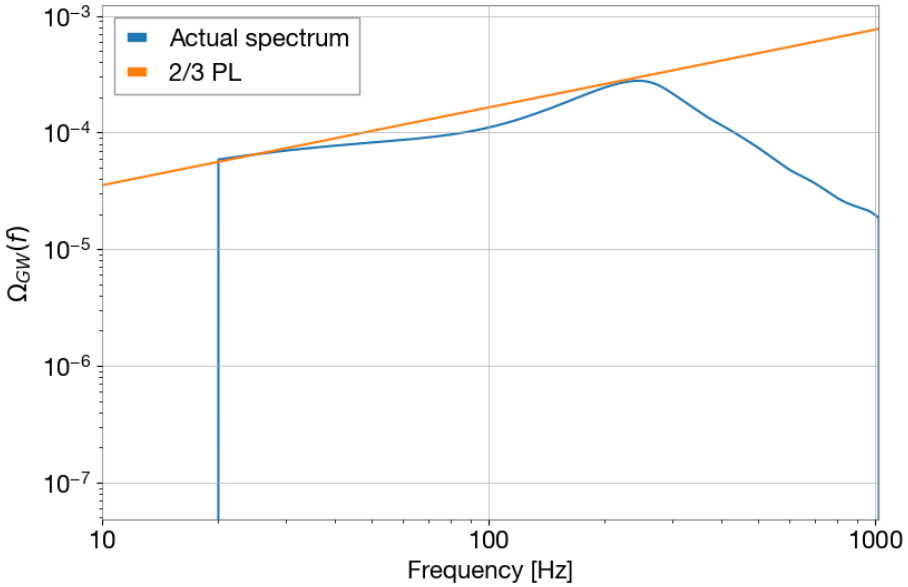

Figure 13: A plot showing how 1000 injections over a frequency range of 10 Hz to 1024 Hz leads to a very smooth curve [18]. The time taken to generate the plot is approximately five minutes, with a 10000-injection dataset taking 30 minutes to plot. Further research may include improving this generation time.

Source: Image generated by the author, but the methodology used can be found through [6, 18].

In the Callister method, all $\Omega_{GW}(f)$ values are in an order of magnitude that is 10^{-10} , while in the Regimbau method, $\Omega_{GW}(f)$ values can be between 10^{-4} to 10^{-8}. We can still see the difference in $\Omega_{GW}(f)$ values by normalizing all inputs — and removing the neutron star contribution from the Callister method — by setting both m_1 and m_2 values to be a minimum of 5 and a maximum of 50 solar masses [17, 18]. We also ensure that both m_1 and m_2 values in the Regimbau method can be described by a normal distribution with a minimum of 5 and a maximum of 50 solar masses [17, 18]. The results of this comparison are shown below in Figure 14 [17, 18]:

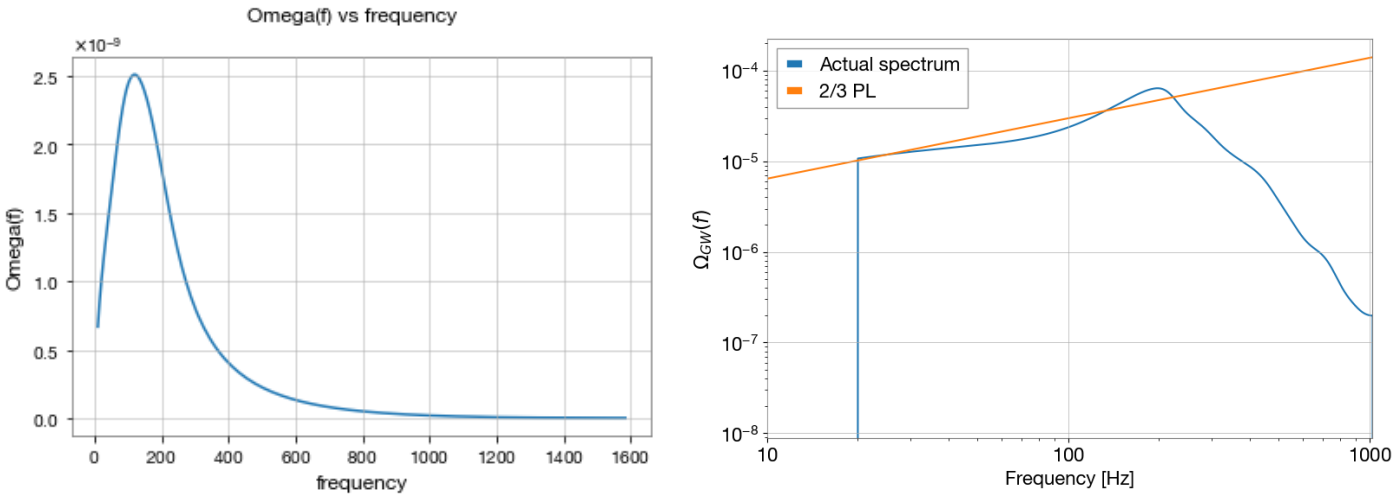

(Left) **(Right)**

Figure 14: The result of the above constraints for both the Callister method (left) and the Regimbau method (right) [17, 18]. As can be seen, while both methods peak at a similar frequency (somewhere in the range of 2×10^2Hz, their peak values, and therefore the entire graphs, fall on entirely different frequency ranges. While the Callister method results in $\Omega_{GW}(f)$ values in a range from 10-8 to 10-9 Hz, the Regimbau method results in $\Omega_{GW}(f)$ values between 10^{-4} to 10^{-8} [17, 18].

Source: Images generated by the author.

This discrepancy is a result of the fact that the observation time and number of injections are separate in the Regimbau method, when in fact, they should be related to each other as per the Callister method. More specifically, the number of injections is proportional to observation time. We can use this fact to calculate the number of injections based on observation time variables used in the Callister's method. We can fine tune for certain values of luminosity distance, set a

common distribution/observation time of one year, and calculate injections from there. With a common mass distribution of 5 to 50 solar masses, we have the comparison plot in Figure 15 below:

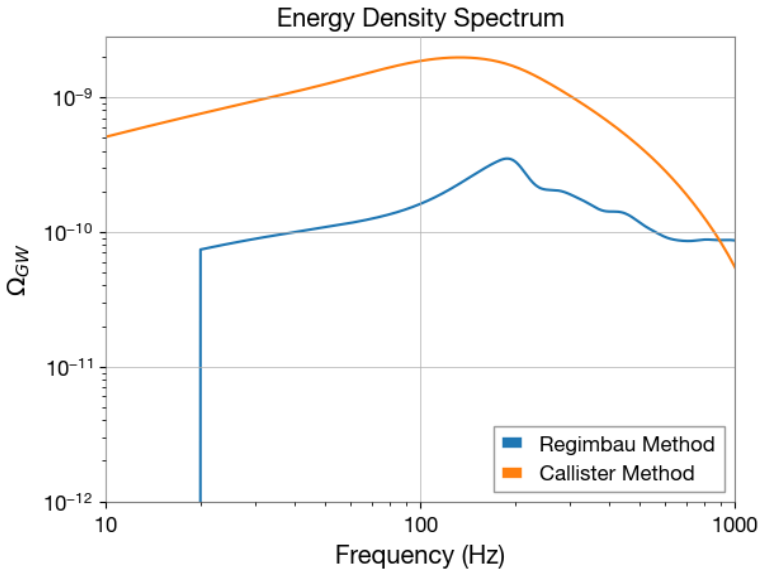

Figure 15: By calculating injections roughly based on a common observation time with the Callister method, we are able to adjust the parameters in the Regimbau method to roughly agree within the same order of magnitude as the Callister method. It should be noted, however, that while the Regimbau method in this case uses a uniform mass distribution — and this can be changed to a power law, broken power law, etc — the Callister method is inbuilt with a power law distribution. Even so, we can still see some agreement between the two methods [17, 18].

Source: Images generated by the author.

We can continue to adjust the observation time in the Callister and Regimbau methods, such that the number of injections matches the appropriate observation time. The result for both m_1 and m_2 with a log distribution of between 5 and 50 solar masses and a redshift distribution from our current redshift of 0 to a redshift of 2 (given by a power law) is shown in Figure 16 [17, 18] below:

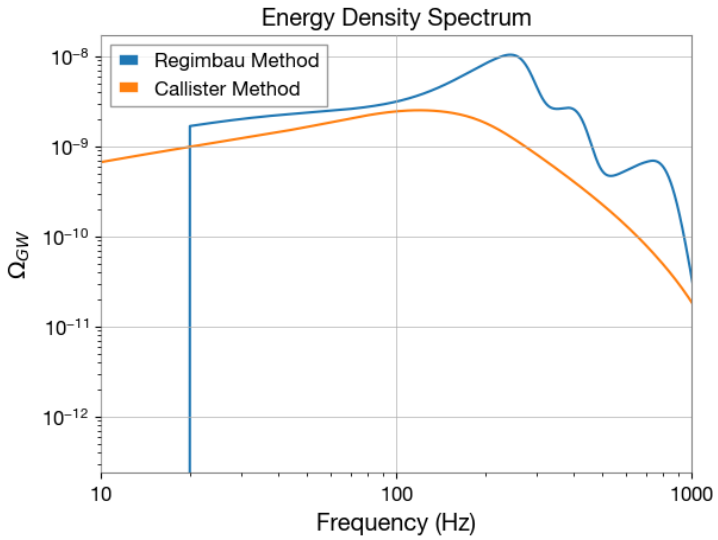

Figure 16: Another attempt is to adjust the observation time for both methods and match the appropriate number of injections to be utilized for the Regimbau method. The two methods now provide results that are close to the same magnitude, suggesting success for this methodology. Instead of using luminosity distance to tune the injections, we use a redshift parameter [17, 18].

Source: Images generated by the author.

Thus, we have managed to temporarily ensure that the two methods agree with one another to at least an order of magnitude. An attempt still needs to be made to fully characterize the injections used in the Regimbau method in terms of the Callister method and observation time. An attempt has also been made on this for the specific observation time of one year, one day, and so on [17, 18].

Next steps and conclusion

As per the section on main objectives, throughout the first part of our research, we have reproduced estimates of energy density of the SGWB from [6] and [7] using corresponding methods in [18] and [17] respectively. By repeating the simulations with different mass distributions and merger rate values, we have decoded the dependance of the estimates on uncertainties in merger rate as a function of mass [17, 18]. We have looked at the degree to which these estimates agree with each other, calculated specific observation times and instances of reasonable agreement between these methods, as well as impacts of uncertainties on potential constraints that can be applied to the SGWB's energy density [17, 18]. We have also initiated the process of inputting priors into the Callister method in the same way that they are utilized in the Regimbau method to allow for a greater comparison between the two methodologies [17, 18].

Our next main goals are to continue generating $\Omega_{GW}(f)$ plots for both the Regimbau and Callister methods, understand the parameter distribution that leads to each plot result, such as merger rate, energy density, frequency etc, and understand how these parameters evolve with differences in mass and redshift distribution [17, 18]. As an example of this pathway of research, recent work has been done on plots of mass distribution of mergers — each represented by a

single mass of the merging pair — for different redshift values to see that as we scale mass distribution with redshift, the cut-off value for mass distribution gets larger and larger.

We define the cut-off as follows: If we plot the change in mass merger rate with redshift against mass values as a power law, we see there is a point where the change in gradient with change in mass is negligible. The mass value that this occurs at, is the cut-off of the mass values. We plot this graph for a red shift of 0 (our reference frame) and a redshift of 2 as shown below in Figure 17. We see that the cut-off values for mass distributions increase with redshift. Further work will need to be completed on breaking down the equations defining the change in merger rate with respect to peak merger mass, the overall probability distribution given particular mass distributions, and how all these values scale with redshift.

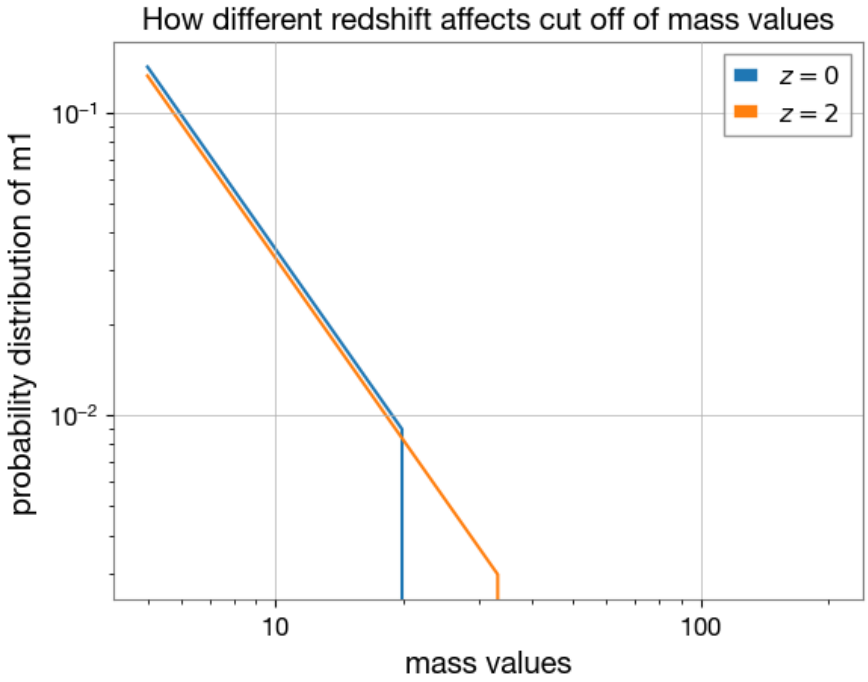

Figure 17: A graph showing how different redshifts affect cut-off values of mass distribution — the point wherein change in mass merger rate for a given change is negligible. This cut-off occurs at higher mass values for higher redshifts.

Source: Images generated by the author.

In any case, the overall goal of this project will be to continue investigating the relationship between various parameters and hyperparameters with changes in mass distribution and redshift distribution. Moreover, a longer-term goal will be to actually use the data collected on SGWB, particularly from recent measurements of the SGWB via supermassive black hole collisions [15]. Overall, the next steps will also be to repeat the same analysis of $\Omega_{GW}(f)$, but measure it as it varies with redshift distribution, thereby looking at the impacts of potential anisotropies.

Bibliography

[1] *LIGO, VIRGO And KAGRA Observing Run Plans,* IGWN, accessed May 2023, https://observing.docs.ligo.org/plan/

[2] *Gravitational Waves from Compact Binary Mergers seen by LIGO and Virgo*, Alan J Weinstein LIGO Laboratory, Caltech for the LIGO and Virgo Collaborations LIGO-Virgo Open Data Workshop, May 27, 2020, https://dcc.ligo.org/public/0168/G2000797/001/Weinstein_CBCs_GWOSC_ODW_20200527.pdf

[3] *Gravitational-wave Transient Catalog (GWTC)*, LVK Collaboration, https://www.gw-openscience.org/eventapi/html/GWTC/

[4] *Stochastic Gravitational-Wave Backgrounds: Current Detection Efforts and Future Prospects*, Renzini, A.I., Goncharov, B., Jenkins, A.C., Meyers, P.M., *Galaxies 2022*, 14 February 2022, https://www.mdpi.com/2075-4434/10/1/34

[5] *Upper limits on the isotropic gravitational-wave background from Advanced LIGO and Advanced Virgo's third observing run*, R. Abbott et al, (LIGO Scientific Collaboration, Virgo Collaboration, and KAGRA Collaboration), *Phys. Rev.* D 104, 022004, Published July 23, 2021, https://journals.aps.org/prd/abstract/10.1103/PhysRevD.104.022004

[6] GW150914: GW150914: *Implications for the Stochastic Gravitational-Wave Background from Binary Black Holes*, B. P. Abbott et al, (LIGO Scientific Collaboration and Virgo Collaboration), *Phys. Rev. Lett.* 116, 131102, Published March 31, 2016, https://journals.aps.org/prl/abstract/10.1103/PhysRevLett.116.131102;
GW170817: *Implications for the Stochastic Gravitational-Wave Background from Compact Binary Coalescences*, B. P. Abbott et al, (LIGO Scientific Collaboration and Virgo Collaboration), *Phys. Rev. Lett*, 120, 091101, Published February 28, 2018, https://journals.aps.org/prl/abstract/10.1103/PhysRevLett.120.091101

[7] *Upper limits on the isotropic gravitational-wave background from Advanced LIGO and Advanced Virgo's third observing run,* R. Abbott et al, (LIGO Scientific Collaboration, Virgo Collaboration, and KAGRA Collaboration), *Phys. Rev. D,* 104, 022004, Published July 23, 2021, https://journals.aps.org/prd/abstract/10.1103/PhysRevD.104.022004, section V.A

[8] *The population of merging compact binaries inferred using gravitational waves through*, GWTC-3, B. P. Abbott et al, (LIGO Scientific Collaboration and Virgo Collaboration), February 23, 2022, https://arxiv.org/abs/2111.03634, section X and Fig 23.

[9] *The stochastic gravitational-wave background from massive black hole binary systems: implications for observations with Pulsar Timing Arrays*, *Monthly Notices of the Royal Astronomical Society*, A. Sesana, A. Vecchio, C. N. Colacino, Volume 390, Issue 1, October 2008, Pages 192-209, https://doi.org/10.1111/j.1365-2966.2008.13682.x

[10] *Introduction To Ligo & Gravitational Waves, Stochastic Gravitational Waves*, LVK Collaboration, https://www.ligo.org/science/GW-Stochastic.php, accessed May 2023

[11] *Impact of a Midband Gravitational Wave Experiment On Detectability of Cosmological Stochastic Gravitational Wave Backgrounds*, Barry C. Barish, Simeon Bird, and Yanou Cui, 16 June 2021, https://arxiv.org/pdf/2012.07874.pdf

[12] *pygwb documentation*, Copyright 2022, Arianna Renzini, Sylvia Biscoveanu, Shivaraj Khandasamy, Kamiel Janssens, Max Lalleman, Katarina Martinovic, Andrew Matas, Patrick Meyers, Alba Romero, Colm Talbot, Leo Tsukada, Kevin Turbang, https://pygwb.docs.ligo.org/pygwb/

[13] *LISA For Cosmologists: Calculating The Signal-To-Noise Ratio For Stochastic And Deterministic Sources*, Tristan L. Smith, Swarthmore College, tsmith2@swarthmore.edu, R. R. Caldwell, 11-15-2019, https://works.swarthmore.edu/cgi/viewcontent.cgi?article=1378&context=fac-physics

[14] *Stochastic gravitational wave background: methods and Implications*, Nick van Remortel, Kamiel Janssens, Kevin Turbang, 3 Oct 2022, https://arxiv.org/abs/2210.00761

[15] *The NANOGrav 15 yr Data Set: Evidence for a Gravitational-wave Background*, Gabriella Agazie et al, Published June 29 2023, DOI: 10.3847/2041-8213/acdac6 https://iopscience.iop.org/article/10.3847/2041-8213/acdac6

[16] *Galaxies from cosmic dawn to cosmic noon with KLASS*, Charlotte Mason, KMOS@5: Star and Galaxy Formation in 3D — Challenges at KMOS 5th Year, Conference held 3-6 December, 2018 in Garching b. München, Germany. Online at https://www.eso.org/sci/meetings/2018/KMOS2018.html, kmos2018, id.23, Publication Date: December 2018, DOI: 10.5281/zenodo.2595152, https://ui.adsabs.harvard.edu/abs/2018kmos.confE..23M/abstract

[17] *Shouts and Murmurs: Combining Individual Gravitational-wave Sources with the Stochastic Background to Measure the History of Binary Black Hole Mergers*, Tom Callister, Maya Fishbach, Daniel E. Holz, Will M. Farr, June 2020, https://ui.adsabs.harvard.edu/abs/2020ApJ...896L..32C, DOI: 10.3847/2041-8213/ab9743. Note, further code outlining the simulation process found at: Thomas Callister, GitHub, https://git.ligo.org/thomas-callister/stochastic-modeling.git (GitHub clone HTTPS), https://git.ligo.org/thomas-callister/stochastic-modeling/-/tree/master/ (main branch link) https://git.ligo.org/thomas-callister/stochastic-modeling/-/tree/master/code (code link and calculation explanation)

[18] *The astrophysical gravitational wave stochastic background*, Tania Regimbau, 2011 National Astronomical Observatories of Chinese Academy of Sciences and IOP Publishing, *Research in Astronomy and Astrophysics*, Volume 11, Number 4, DOI 10.1088/1674-4527/11/4/001, https://iopscience.iop.org/article/10.1088/1674-4527/11/4/001. Note, further code outlining simulation process found at: Arianna Renzini, GitHub, https://git.ligo.org/pygwb/pygwb.git (GitHub clone HTTPS), https://git.ligo.org/arianna.renzini/pygwb-ssi/-/tree/master/tutorials (main list of tutorials

followed), https://git.ligo.org/arianna.renzini/pygwb-ssi/-/tree/master/pygwb (for simulating a CBC background)